2

Conf-941011--5

SAND93-2698C

Paper to be presented at:
3rd International Conference on Containment Design and Operation
Toronto, Canada
October 19-21, 1994

ANALYSES OF A STEEL CONTAINMENT VESSEL WITH AN OUTER CONTACT STRUCTURE UNDER SEVERE INTERNAL OVERPRESSURIZATION CONDITIONS*

Vicki L. Porter

ABSTRACT

Many Mark-I and Mark-II BWR plants are designed with a steel vessel as the primary containment. Typically, the steel containment vessel (SCV) is enclosed within a reinforced concrete shield building with only a small gap (50-90mm) separating the two structures. This paper describes finite element analyses performed to evaluate the effects of contact and friction between a steel containment vessel and an outer contact structure when the containment vessel is subjected to large internal pressures. These computations were motivated by a joint program on containment integrity involving the Nuclear Power Engineering Corporation (NUPEC) of Japan, the US Nuclear Regulatory Commission (NRC), and Sandia National Laboratories for testing model containments.

Under severe accident loading conditions, the steel containment vessel in a typical Mark-I or Mark-II plant may deform under internal pressurization such that it contacts the inner surface of a shield building wall. (Thermal expansion from increasing accident temperatures would also close the gap between the SCV and the shield building, but temperature effects are not considered in these analyses.) The amount and location of contact and the pressure at which it occurs all affect how the combined structure behaves. A preliminary finite element model has been developed to analyze a model of a typical steel containment vessel coming into contact with an outer structure. Both the steel containment vessel and the outer contact structure were modelled with axisymmetric shell finite elements. Of particular interest are the influence that the contact structure has on deformation and potential failure modes of the containment vessel. Furthermore, the coefficient of friction between the two structures was varied to study its effects on the behavior of the containment vessel and on the uplift loads transmitted to the contact structure. These analyses show that the material properties of an outer contact structure and the amount of friction between the two structures can have a significant effect on their behavior.

*This program is sponsored by the Nuclear Power Engineering Corporation (NUPEC) of Japan and the U. S. Nuclear Regulatory Commission. The work was performed at Sandia National Laboratories, supported by the U.S. Department of Energy under Contract DE-AC04-94AL85000.

DISCLAIMER

Portions of this document may be illegible in electronic image products. Images are produced from the best available original document.

ANALYSES OF A STEEL CONTAINMENT VESSEL WITH AN OUTER CONTACT STRUCTURE UNDER SEVERE INTERNAL OVERPRESSURIZATION CONDITIONS

Vicki L. Porter

1. INTRODUCTION

Many Mark-I and Mark-II BWR plants are designed with a steel vessel as the primary containment. Typically, the steel containment is enclosed within a reinforced concrete shield building with only a small gap between the two structures. Under severe accident loading conditions, the deformation of the steel containment vessel (SCV) under internal pressurization and high temperatures may be such that contact occurs between the outer surface of the SCV and the inner surface of the shield building. Only the effects of overpressurization are analyzed in this paper; temperature effects are not considered.

As part of a joint program with the Nuclear Power Engineering Corporation (NUPEC) of Japan and the US Nuclear Regulatory Commission (NRC), Sandia will pressurize a scale model of a BWR Mk-II steel containment vessel up to failure to develop a database for checking analytical modeling methods. A scale of 1:10 will be used for the SCV model, except that the wall thickness will be 1:4 scale. A "contact structure" will be placed around the SCV model in order to gain insight on the effects of contact on the SCV model behavior. The design of the contact structure is currently underway.

This paper describes preliminary scoping analyses of the SCV model and two different representations of an outer contact structure. In the first case, the contact structure was elastic with a very large stiffness so that it represented a nearly rigid barrier. In this case, the contact was assumed to be frictionless. In the second representation, the contact structure was modeled with an elastic-plastic material. Two analyses, with and without friction between the containment vessel and the contact structure, were conducted with the elastic-plastic representation.

2. MODEL DESCRIPTION

The finite element representation of the SCV model with the contact structure is shown in Figure 1. The finite element model utilized two-node axisymmetric shell elements for the containment vessel and contact structure walls, ring stiffeners, and rings of the support girder. Five integration points were used through the shell thickness. Flanges and gusset plates used for stiffeners of the ring support girder were modeled with four-node axisymmetric quadrilaterals. Pressure was applied to the entire interior surface of the SCV model. The contact structure is only loaded through contact with the SCV model and its connection to the ring support girder. Contact between the two structures was modeled with two-node, axisymmetric slide line elements superimposed on the SCV model shell elements. It must be noted that because this is a shell model, contact is only de-

tected when the shell midsurfaces intersect. This assumption is valid as long as the variations in shell thickness are negligible compared to the gap size. When contact is detected between the nodes of these elements and the elements on the contact structure, a stress is induced in the slide line elements in the direction of the normal. A tangential stress is also introduced if a non-zero coefficient of friction is specified. All computations were performed with the commercial finite element code, ABAQUS [1].

The SCV model is constructed of SPV 490 and SGV 480 steels. Because test data for the actual materials used in the model are not yet available, previously reported values from the published literature [2] were used. The reported stress-strain behavior for these two materials was converted to true stress and true strain only up to the point of maximum load since conversion beyond this point is not possible without the reduction in cross-sectional area at the point of necking in the sample.

3. RESULTS

The purpose of these analyses was to characterize the influence of contact friction and the material properties of the contact structure on the behavior of the SCV model. Three different representations of a contact structure were analyzed. In the first case, the contact structure was given a very high modulus of elasticity to simulate a nearly rigid structure (hereafter referred to as the "rigid" contact structure) for a lower bound on displacements. Friction between the SCV model and the rigid structure was assumed to be zero. In the second analysis, the contact structure was assumed to be constructed of elastic-plastic steel "hereafter referred to as the "flexible" contact structure. In this case, the friction between the SCV and the flexible contact structure was again assumed to be zero. In the third and final analysis, the coefficient of friction was taken to be 0.25 between the SCV and the flexible contact structure.

In all the results presented here, the final pressure is the highest pressure at which the code could converge with a reasonable pressure step. The code fails to converge because the strain at some point has reached the maximum defined in the material models throughout the shell wall thickness. In these analyses the maximum defined strain of the material model is approximately 15%. This is a result of the fact that the material data available was converted from engineering stress-strain data to true stress-strain data, the relationships for which are only valid up to the point of maximum load in a tensile test. Due to these limitations in material data, the maximum internal pressure in these preliminary computations should not be interpreted as a failure pressure.

3.1 Contact Initiation

Under internal pressurization, the SCV model expands and eventually contacts the surrounding contact structure. However, due to stiffening rings and variations in SCV wall thickness, not all portions of the model contact the outer structure at the same pressure. The table in Figure 2 shows the internal pressure at which contact occurs for the rigid and flexible contact structures at various locations of the SCV model. Because the internal pressure at which contact occurs was the same for the flexible contact structures at all locations, only one column is shown for the flexible struc-

tures. That is, the amount of friction present between the SCV model and the contact structure had no effect on the pressure at which contact first occurs. No contact occurred between the contact structure and the top head of the SCV model above the knuckle region in any of the analyses.

For both the rigid and the flexible structures, contact first occurs in the knuckle region at an internal pressure between 3.1 and 3.3 MPa. It must be noted, however, that the elements used in these analyses are shell elements with no physical thickness. Contact is only detected when the middle surface of the SCV shell wall reaches the middle surface of the contact structure. Because the knuckle region is much thicker than the rest of the SCV model, contact will actually occur earlier than that shown by the shell element analyses. Contact in the knuckle region is followed almost immediately by contact in both the upper and lower conical sections. In both cases, this contact initiates in the center of the two regions, i.e. approximately equidistant between the ring stiffeners. The contact region then continues to expand uniformly in the conical regions until an internal pressure of 5.5MPa is reached, at which time the spherical region between the conical sections and the knuckle makes contact. Finally, the wet well region contacts the contact structure at an internal pressure between 6.5 and 6.7MPa.

As indicated in Figure 2, there is very little difference in the values of the internal pressure when contact occurs for the rigid and flexible contact structures. In fact, the minor differences shown in the table for the spherical and wet well regions are probably a consequence of slightly different pressures at which output was obtained rather than real differences in contact. The similarity in the pressures for the two contact structure representations indicates that the rigidity of the contact structure has little effect on radial deformations of the SCV model up to the point of contact. Of course, once contact occurs, the stiffness of the contact structure can be expected to have a significant effect on the radial deformation of the combined structure.

3.2 Top Head and Knuckle Region

Results for the SCV response in the top head and knuckle regions are shown in Figures 3 through 11. As shown in Figure 3, the vertical displacement at the apex of the top head is the same for all three contact structures up to an internal pressure of 5.0 MPa. This is approximately the pressure at which full contact is achieved between the SCV model and the contact structure along the entire surface from the knuckle down to the top of the wet well. Therefore, above this pressure the effects of friction and the rigidity of the contact structure become more noticeable. Beyond an internal pressure of 11.0 MPa, the vertical displacement increases very rapidly for all three cases due to extensive yielding near the center of the top head. Note that the maximum displacement at the apex of the top head is 130mm, which is less than the gap in this region (see Figure 1) so no contact with the outer structure occurs here.

The equivalent plastic strain, defined as $\varepsilon^p = \sqrt{(2/3)\,\varepsilon^p_{ij}\varepsilon^p_{ij}}$, is shown in Figure 4 for the apex of the top head. The plastic strain is the same for all three analyses at any internal pressure, with yielding predicted at an internal pressure of 5.2MPa. Neither the rigidity of the contact structure nor the coefficient of friction between the model and the contact structure seem to influence the strain state at the apex of the top head.

The knuckle region is an area of transition from a spherical shape into the cylindrical shape of the top head. The knuckle itself is over twice as thick as the surrounding wall thickness making this an area of stress concentration. A detailed view of this region including element numbers is shown in Figure 5. The knuckle itself is comprised of elements 130 to 139. Because shell elements are used, the contrast in thickness cannot be seen in the finite element mesh. However, at its thickest point, the knuckle is 16.5mm thick, while the spherical wall below is 8mm thick, and the cylindrical wall above is only 6mm thick.

Figures 6 to 8 show the distribution of equivalent plastic strain in the knuckle region at first yield, at an intermediate pressure, and at the final pressure. As shown in Figure 6, yield initiates in the knuckle region in elements 129 to 137 at an internal pressure of 2.76MPa for all three contact structure representations. By the time the pressure has increased to 6.0MPa (Figure 7), significant differences in the three cases can be seen. The more flexible, frictionless contact structure allows more deformation than the frictionless rigid structure so the plastic strains are generally higher. However, the effect of friction is to couple the tangential (meridional) deformation of the SCV model to that of the contact structure, thereby reducing the meridional strain and, consequently, the total equivalent plastic strain. In all three cases, the maximum plastic strain in this region occurs just below the top head flange in element 149. Local peaks occur above and below the thickened knuckle in elements 140 and 129, respectively. These same elements also show local peaks in plastic strain at an internal pressure of 11.6MPa as shown in Figure 8. However, at this higher pressure, the SCV model with a rigid contact enclosure experiences a sharp increase in plastic strain in elements 133 and 134 of the knuckle itself, while the elements on either side are at a lower strain than the same elements in the two models with a flexible contact structure.

The history of plastic strain, hoop membrane strain, and meridional bending strains for element 140 located immediately above the knuckle are plotted in Figures 9 to 11. It is evident from Figure 9 that both friction and contact structure rigidity play a significant role in the accumulation of plastic strain in this element. The strain is the lowest in the SCV model with a rigid contact structure. The case showing the highest plastic strain is that of the flexible contact structure with a non-zero coefficient of friction. For all three contact structure representations, the deformation of element 140 is influenced by the contact between the knuckle of the SCV model and the lip of the contact structure, although this element is not itself in contact. Larger deformation occurs in the model with non-zero friction than the model without friction because the friction in the knuckle contact constrains the elements in the knuckle from tangential motion. Therefore, the deformation is more concentrated in the element just above the knuckle in the case of non-zero friction coefficient. The largest difference between the frictionless representations is seen in the hoop strain component plotted in Figure 10 because this strain is heavily influenced by the contact structure rigidity in the knuckle region. On the other hand, the largest difference in meridional bending strain occurs due to the influence of friction as shown in Figure 11. While this strain component is about the same for the two frictionless structures, it is significantly higher for the case of non-zero friction. Comparison of the strain magnitudes in Figures 10 and 11 illustrates that the major component of the plastic strain in element 140 is the meridional bending strain, especially in the analysis with a flexible contact structure and non-zero friction coefficient.

3.3 Conical Section

Because the contact structure will have an opening around the sleeve of the equipment hatch, the vertical displacement at the equipment hatch will determine whether contact occurs between the cut-out of the contact structure and the sleeve of the equipment hatch. The analyses described here are all axisymmetric, so the equipment hatch was not explicitly included in the finite element model. However, its location is indicated in Figure 1. Figure 12 compares the vertical displacements for the three contact structure representations at the point on the SCV model corresponding to the top of the equipment hatch. The frictionless flexible contact structure allows only slightly more deformation of the SCV model at this point than the frictionless rigid structure. However, the effect of friction is significant. In the presence of friction, the direction of the final vertical displacement of the point at the top of the equipment hatch is reversed. The dramatic difference between contact with and without friction for internal pressures higher that 5.0MPa is mainly due to deformations occurring in the wet well at these pressures. The wet well yields and experiences large radial expansion at pressures beyond 5.0 MPa. The gap in this area is much larger than in the sections above (Figure 1). Thus, the outer movement of the wet well tends to pull down the upper portions of the SCV. In the case of no friction, the wet well deformation causes the vertical displacement of the equipment hatch to reverse direction and even to go negative. In the case of non-zero friction, however, the contact between the SCV model and the contact structure provides constraint against this tangential downward motion. For the assumed friction coefficient of 0.25, the equipment hatch actually moves upward following the general shell deformation of the contact structure.

The displacement of the equipment hatch relative to a point on the contact structure at the same initial elevation indicates whether contact will occur between the equipment hatch sleeve and the opening in the contact structure. This relative displacement is plotted in Figure 13. The relative vertical displacement for the rigid contact structure in Figure 13 is the same as the absolute vertical displacement for the same case in Figure 12 because, by definition, the rigid contact structure does not deform. For the frictionless, flexible contact structure, the sleeve of the equipment hatch moves downward almost 11mm relative to the contact structure even though its absolute motion is only downward 7.5mm. This means that, in the absence of friction, if the gap between the equipment hatch sleeve and the contact structure sleeve is less than 11mm, contact will occur on the bottom side of the equipment hatch. For a friction coefficient of 0.25, however, the displacement of the SCV equipment hatch sleeve is upward relative to the contact structure. In this case, the relative displacement reaches a maximum of less than 3mm at 5.0MPa internal pressure and levels off to 2mm after 7MPa. Beyond 7MPa, the relative displacement of the SCV model is constant indicating that the SCV model and contact structure are deforming together. These results indicate that contact between the equipment hatch sleeve and the contact structure sleeve is much less likely when friction is present between the two structures. Furthermore, if contact did occur, it would be on the top side of the equipment hatch sleeve.

Figure 14 shows the plastic strain deformation in the lower conical section, which includes the equipment hatch, at two different internal pressures. At 5.06MPa, there is little difference between the three contact structure representations. Recall that contact with the contact structure first occurs at 3.7MPa. The sharp increase in strain between 0.6m and 0.7m is due to both a decrease in the shell wall thickness from 9.0mm to 8.5mm and a change in materials from SPV 490 to SGV 480

steel. At the higher pressure of 11.6MPa, significant differences in plastic strain are apparent for the different contact structure representations although the maximum strain is less than 2%. Larger strain occurs in the analyses with the flexible contact structure than that with a rigid structure because the contact structure is allowed to deform. In addition, the strain is the highest for the zero friction case because the vertical deformation of the containment vessel is not coupled with that of the contact structure through a tangential contact force induced by friction.

4. Wet Well Section

Figure 15 shows the finite element discretization of the wet well area of the SCV model. The upper mesh shows the elements in the area where the SCV model transitions from the cylindrical wet well to the lower conical wall section, and the lower mesh shows that transition from the very thick spherical bottom head to the cylindrical wall of the wet well. Element 200 is the last element of the bottom head and element 1 is the first element of the SCV model wet well. Element 264 is the first element of the contact structure where it attaches to the exterior ring support girder.

Distribution of equivalent plastic strain in the wet well at two different internal pressures is shown in Figure 16. Yielding first occurs in the first element in the conical shell wall above the cylindrical wet well (element 26) at an internal pressure of 3.67MPa for all three contact structure representations. At an internal pressure of 5.06MPa, the results are identical for all three analysis cases. The maximum strain occurs in element 26, and a local maximum with a lower value occurs in element 9 near the center of the wet well. However, at 11.6MPa, the maximum equivalent plastic strain in element 9 is 5 to 7% compared to the local maximum in element 26 of only 3 to 4%. Furthermore, at the higher pressure, the results for the two frictionless contact structures indicate significantly lower plastic strains than the results for the non-zero friction case.

Figure 17 shows the hoop strain component in the wet well. The results indicate identical response of the wet well for the three contact structure representations at an internal pressure of 5.06Mpa. However, even though the non-zero friction case showed a higher plastic strain at 11.6MPa than the frictionless contact structure representations, the results plotted in Figure 17 show a lower hoop strain in the case of non-zero friction. The explanation of higher plastic strain in the case of a non-zero friction coefficient is that the meridional bending strains (shown in Figures 18 and 19) are a large portion of the total strain, and these components are higher for non-zero friction than for the frictionless cases. Figures 18 and 19 show that the meridional bending strain is larger for the case of non-zero friction at both the interior and exterior surfaces of the shell.

5. Uplift Force on Ring Support Girder

The amount of uplift that the contact structure imparts to the outer ring support girder can be estimated knowing the meridional stress in the contact structure at a point immediately above the support. Multiplying the meridional membrane stress by the cross-sectional area of the contact structure of the element just above the support girder (element 264 in Figure 15) gives the total uplift load. Figure 20 shows the uplift force for the two flexible structures. (The force in the "rigid" structure is meaningless.) This is the total force exerted on the entire circumference of the ring. The re-

sults plotted in Figure 20 indicate that the effect of friction is to reduce the uplift force on the ring support girder. This reduction in the presence of non-zero friction occurs due to coupling of downward motion of the wet well under large plastic deformation with the contact structure.

6. SUMMARY

This paper describes results of preliminary axisymmetric analyses designed to investigate the effects of friction and material properties of a contact structure to be included the NUPEC/USNRC/ Sandia containment test program for the SCV model. Three representations of a contact structure were analyzed--a rigid frictionless contact structure, a flexible frictionless contact structure, and the same flexible contact structure with a coefficient of friction of 0.25 between the SCV model and the contact structure. In all three cases, the finite element code failed to converge beyond an internal pressure of 11.6MPa due to large plastic flow at the center of the top head.

The effects of friction during contact between the SCV model and the contact structure are most apparent in the results for vertical displacement of a point corresponding to the location of the equipment hatch. At this location the two frictionless analyses indicate that the equipment hatch displaces downward at a nearly constant rate for internal pressures above 6.0MPa due to large radial expansion in the wet well below. However, when friction was included in the model, this same point actually displaced upward and then became constant for pressures above 6.0MPa. Therefore, if and where contact occurs between the equipment hatch sleeve and the opening through the contact structure are strongly dependent on the amount of friction between the two structures.

Finite element results indicated that the effect of friction was to cause higher plastic strain in the wet well section of the SCV model. This effect is mainly due to higher meridional bending strains when there is a non-zero coefficient of friction between the SCV model and the contact structure. At the same time, the presence of non-zero friction resulted in a lower uplift force from the contact structure wall onto the outer ring support girder.

7. REFERENCES

1. ABAQUS, Version 5.2, Hibbitt, Karlsson and Sorensen, Inc., Pawtucket, RI, 1993.

2. T. Isozaki, K. Soda, S. Miyazono, "Structural Analysis of a Japanese BWR MARK-I Containment under Internal Pressure Loading," **Proceedings of the Third Workshop on Containment Integrity**, NUREG/CP-0076, SAND86-0618, August, 1986.

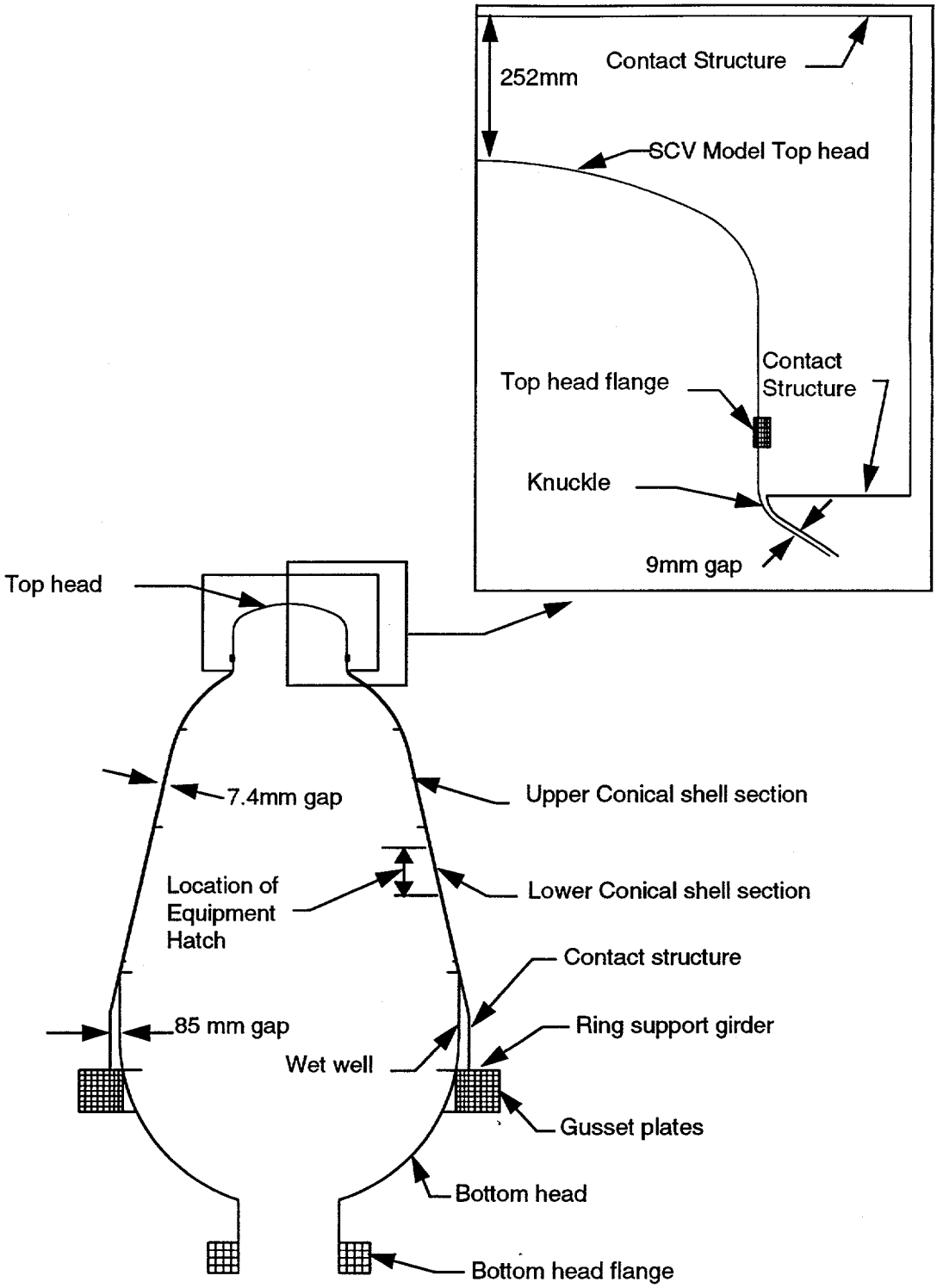

Figure 1. Axisymmetric finite element model of SCV with steel surrogate at representative gap from undeformed SCV.

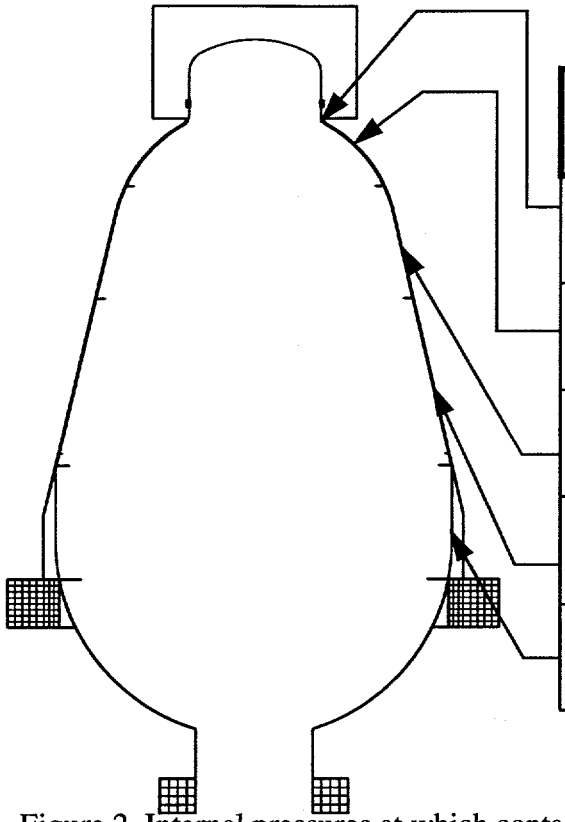

Internal Pressure at Contact (MPa)

Region	Rigid	Flexible
Knuckle	3.1--3.3	3.1--3.3
Spherical	5.5--6.0	5.8--6.0
Upper Conical	3.3--3.7	3.3--3.7
Lower Conical	3.3--3.7	3.3--3.7
Wet Well	6.5--6.7	6.3-6.6

Figure 2. Internal pressures at which contact occurs for various locations.

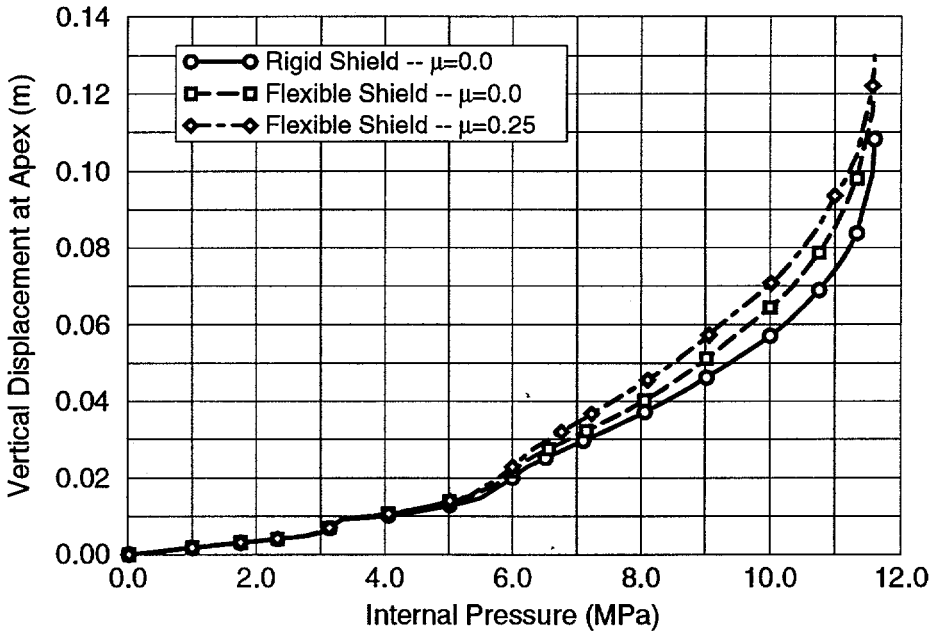

Figure 3. Vertical displacements at apex of top head.

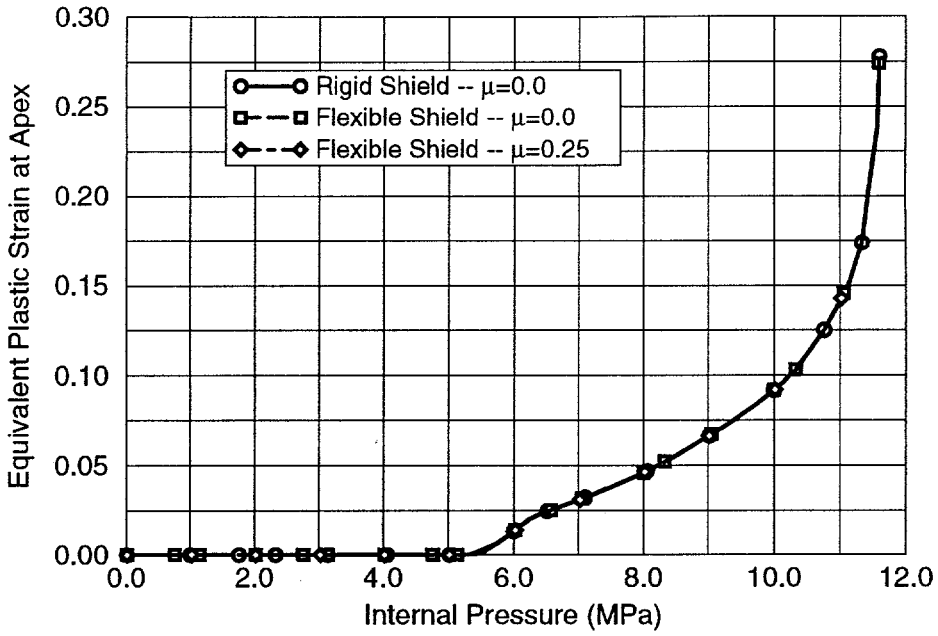

Figure 4. History of equivalent plastic strain at the apex of the top head.

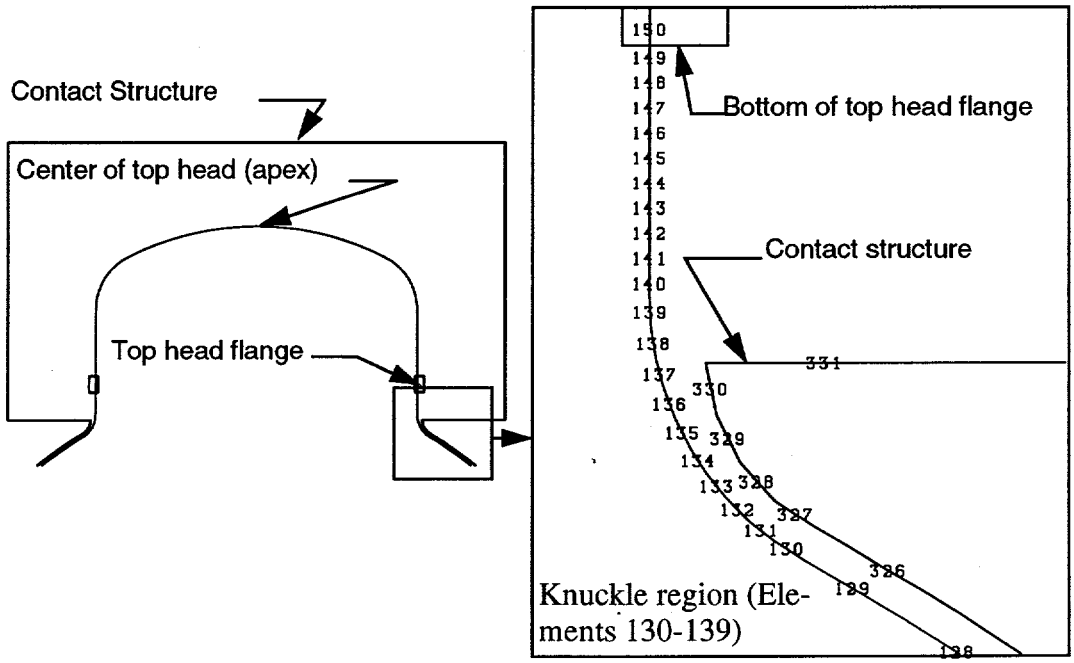

Figure 5. Finite element discretization of top head and knuckle region.

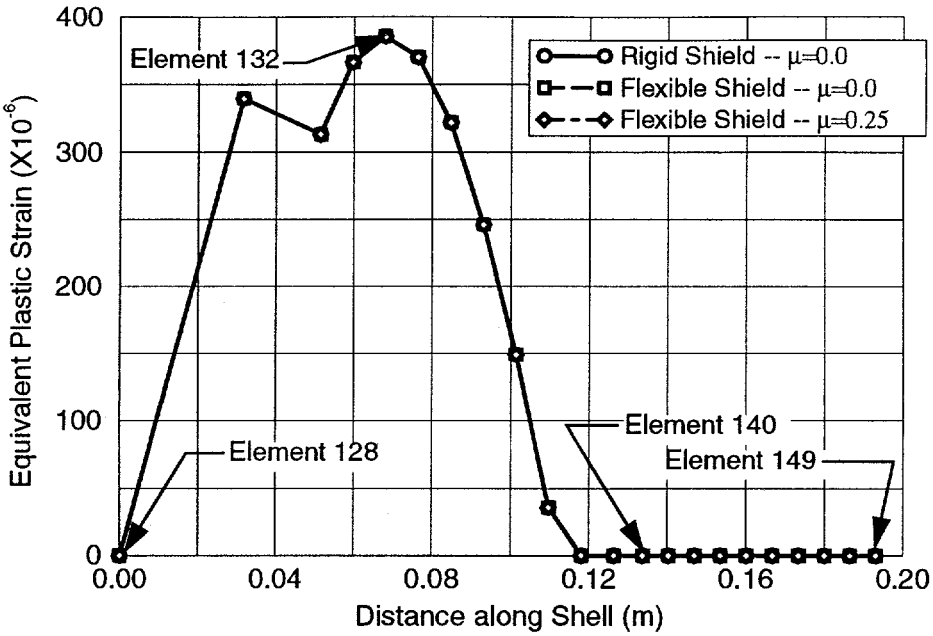

Figure 6. Distribution of plastic strain in knuckle region at an internal pressure of 2.76MPa (first yield in knuckle region).

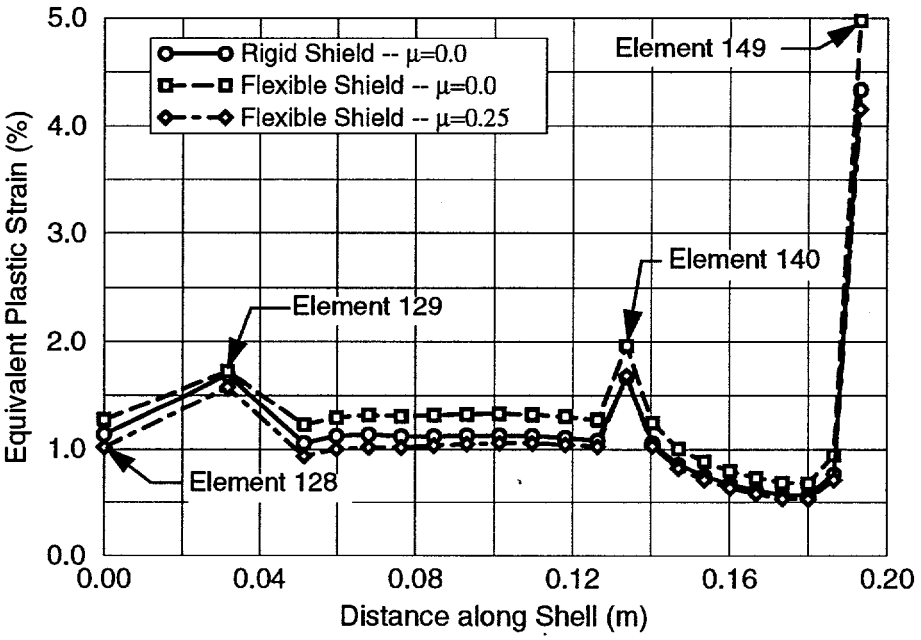

Figure 7. Distribution of plastic strain in knuckle region at an internal pressure of 6.0MPa.

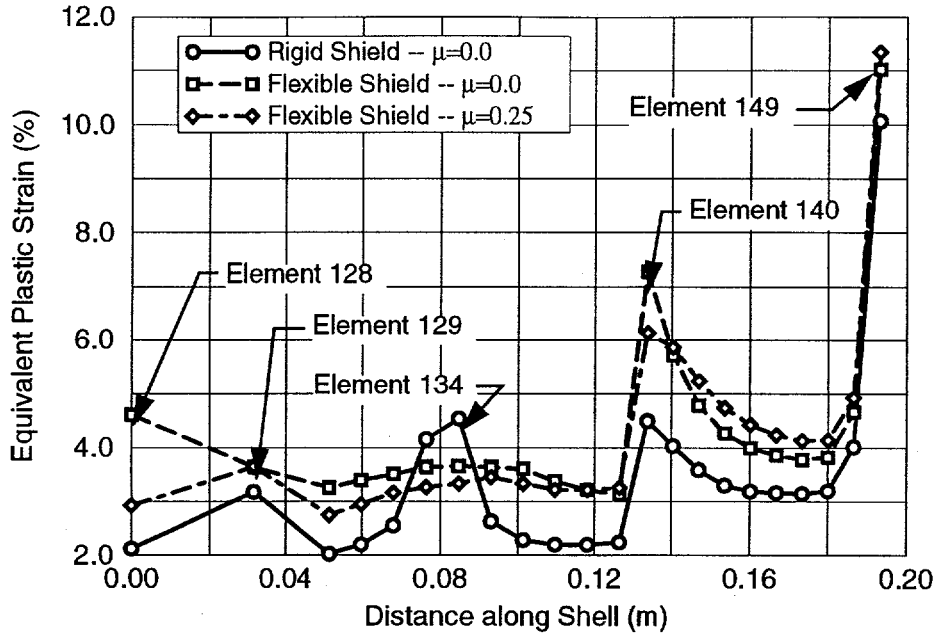

Figure 8. Distribution of plastic strain in knuckle region at an internal pressure of 11.6MPa.

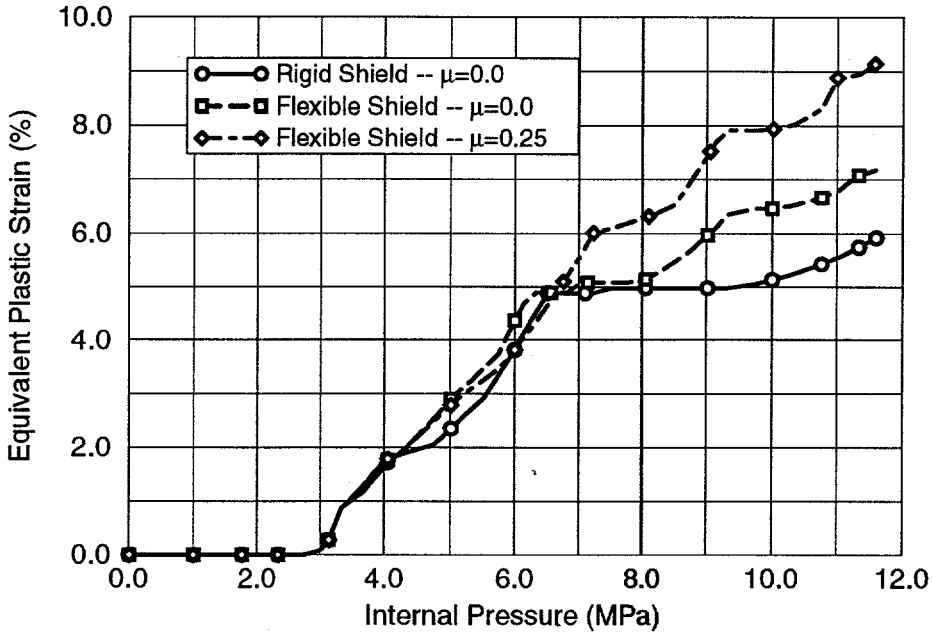

Figure 9. Equivalent plastic strain at a point immediately above knuckle (element 140).

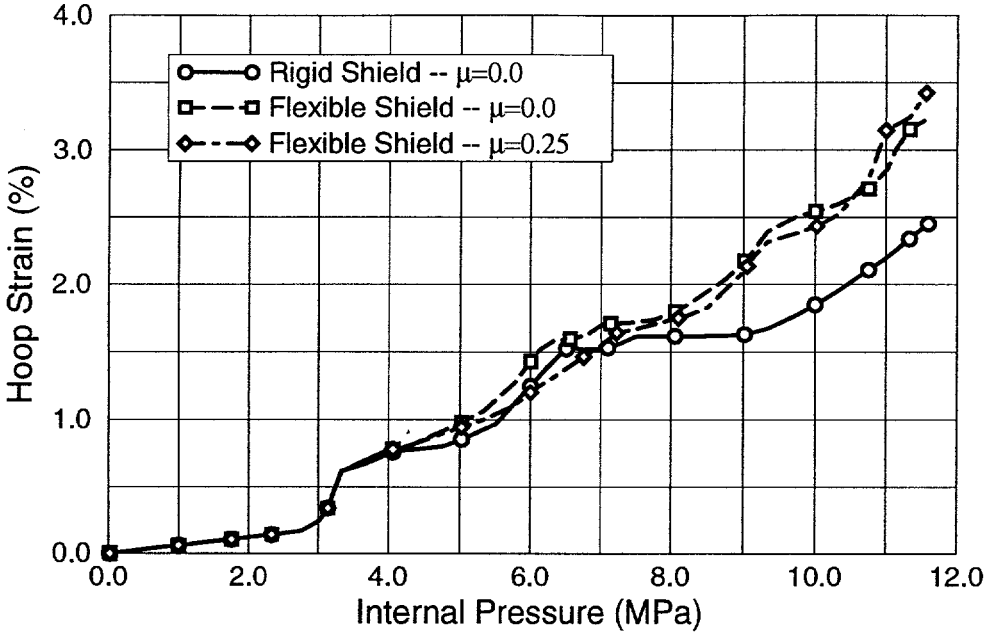

Figure 10. Hoop strain history for point immediately above knuckle (element 140).

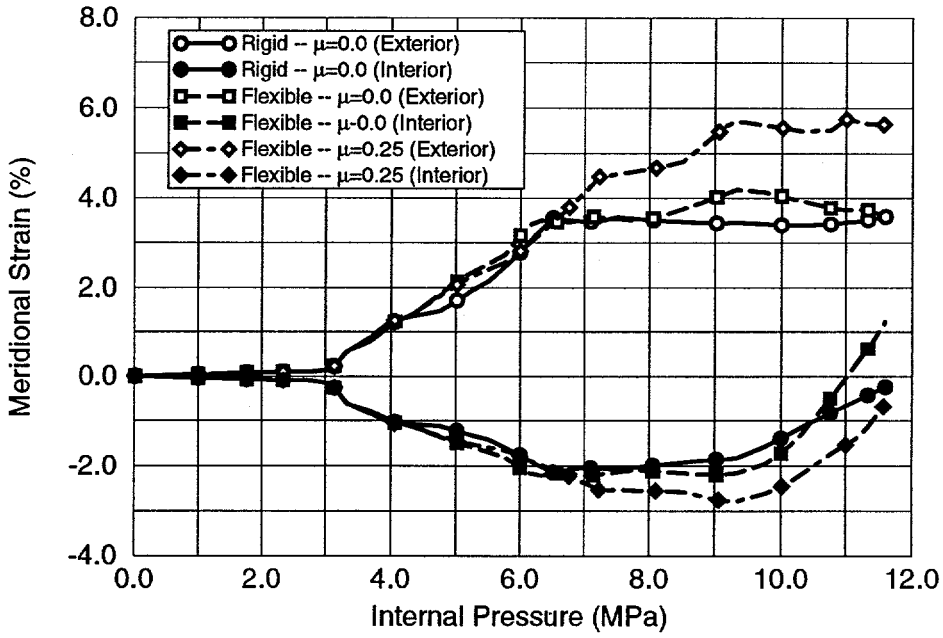

Figure 11. Meridional bending strains immediately above knuckle (element 140).

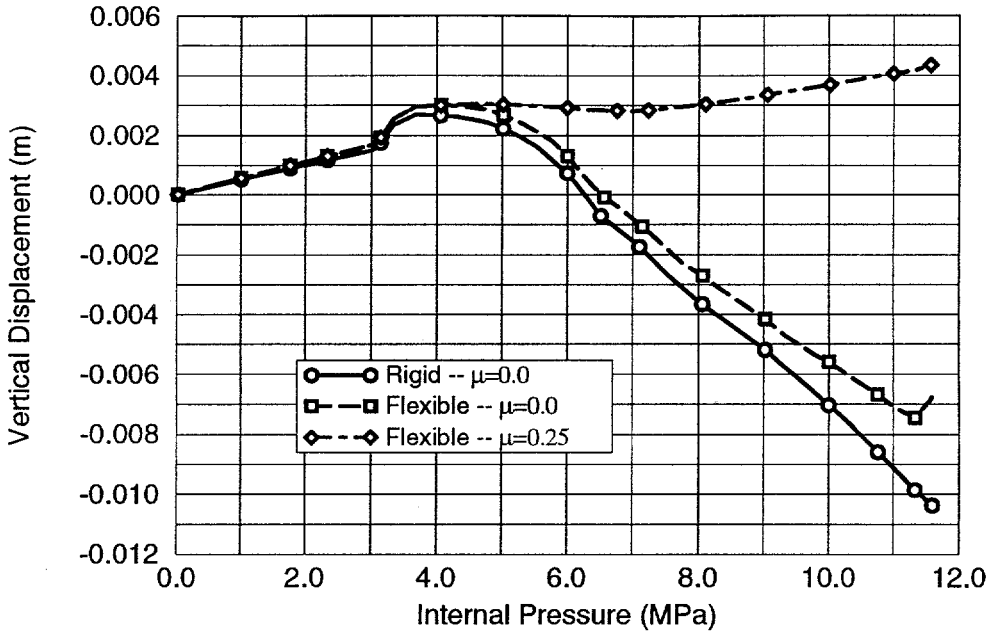

Figure 12. Actual displacement of top of equipment hatch.

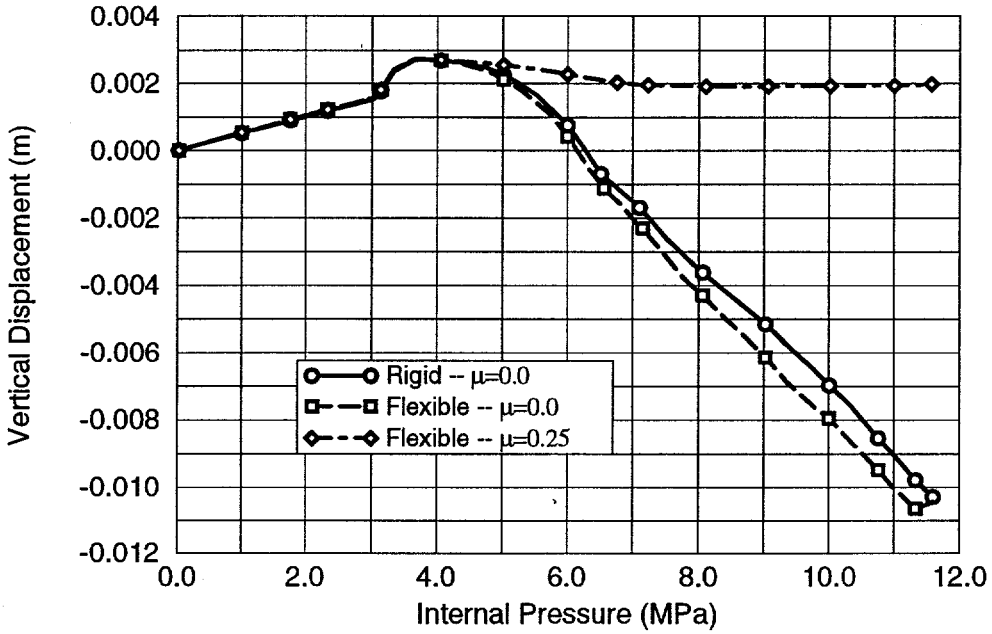

Figure 13. Displacement of top of equipment hatch relative to point on contact structure at same initial elevation.

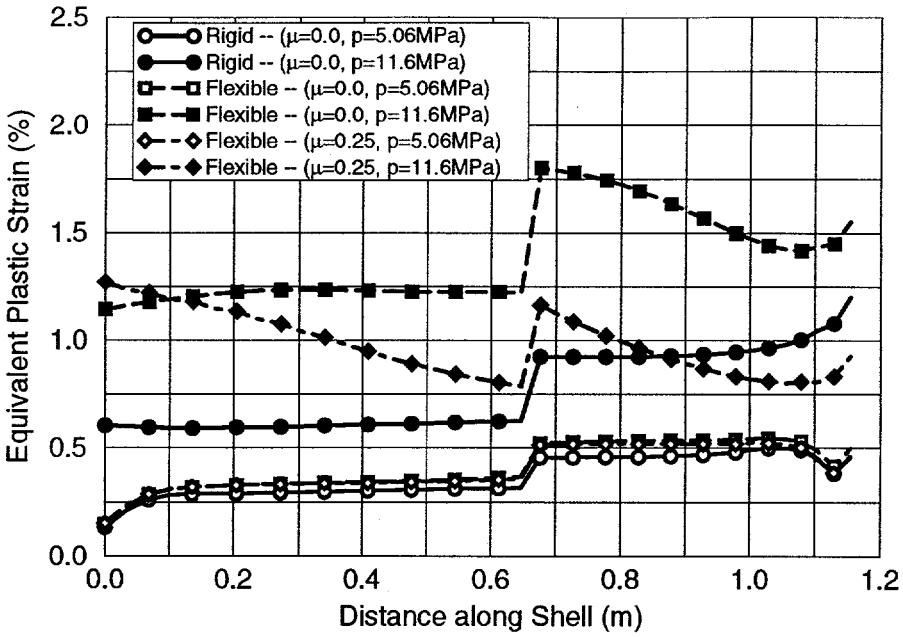

Figure 14. Equivalent plastic strain distribution in lower conical section at internal pressures of 5.06 and 11.6MPa.

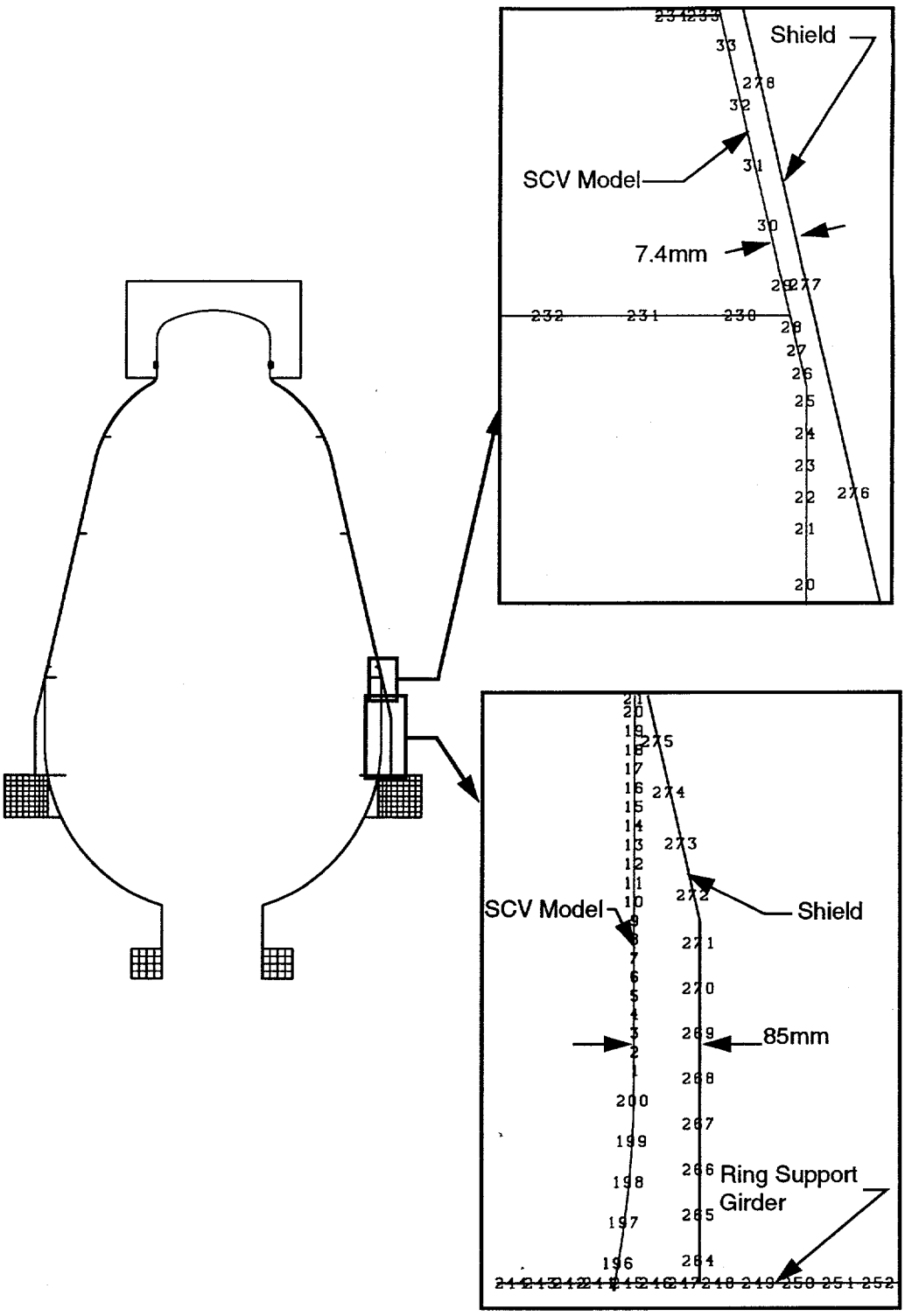

Figure 15. Finite element discretization of wet well section.

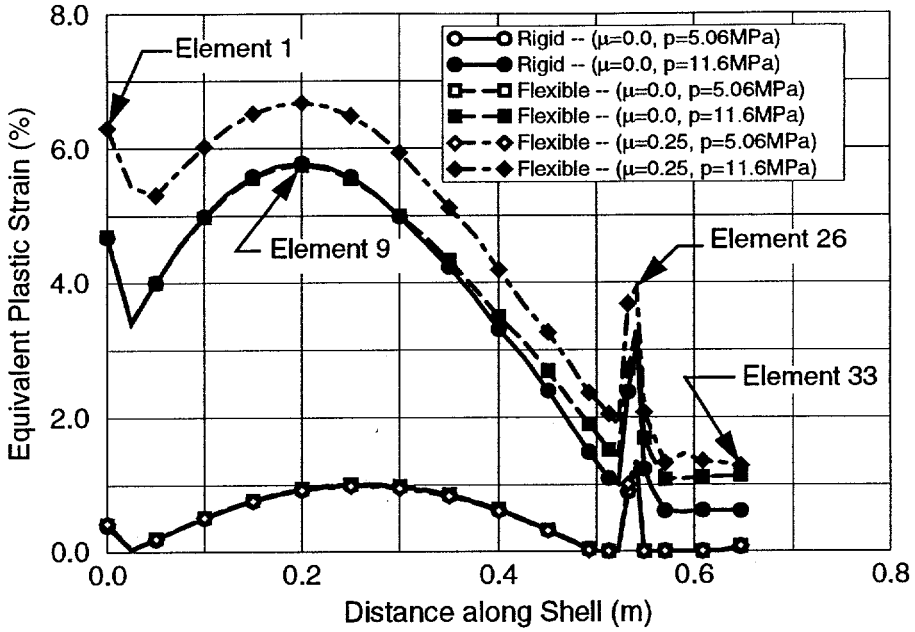

Figure 16. Equivalent plastic strain in wet well at internal pressures of 5.06 and 11.6MPa.

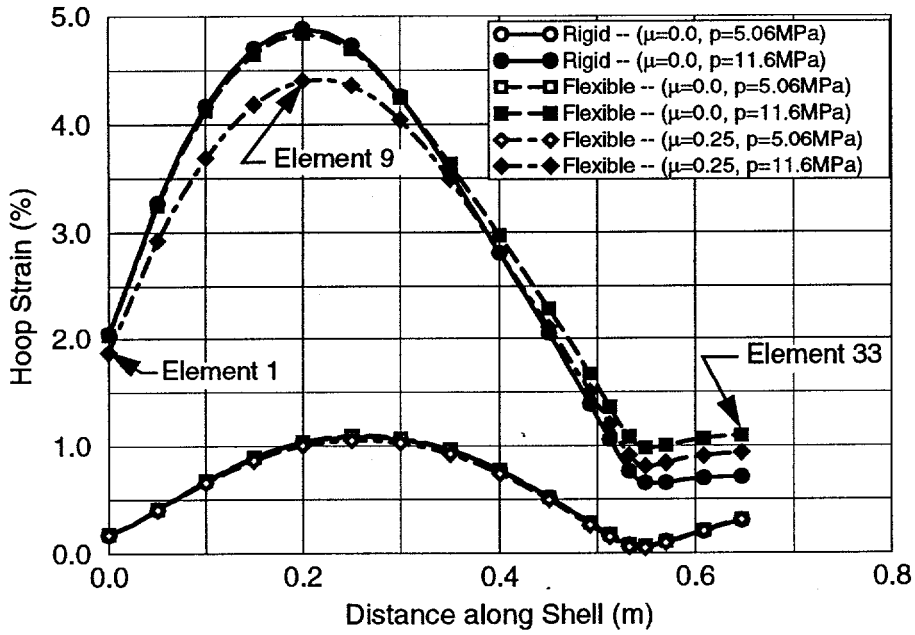

Figure 17. Hoop strain in wet well at internal pressures of 5.06 and 11.6MPa.

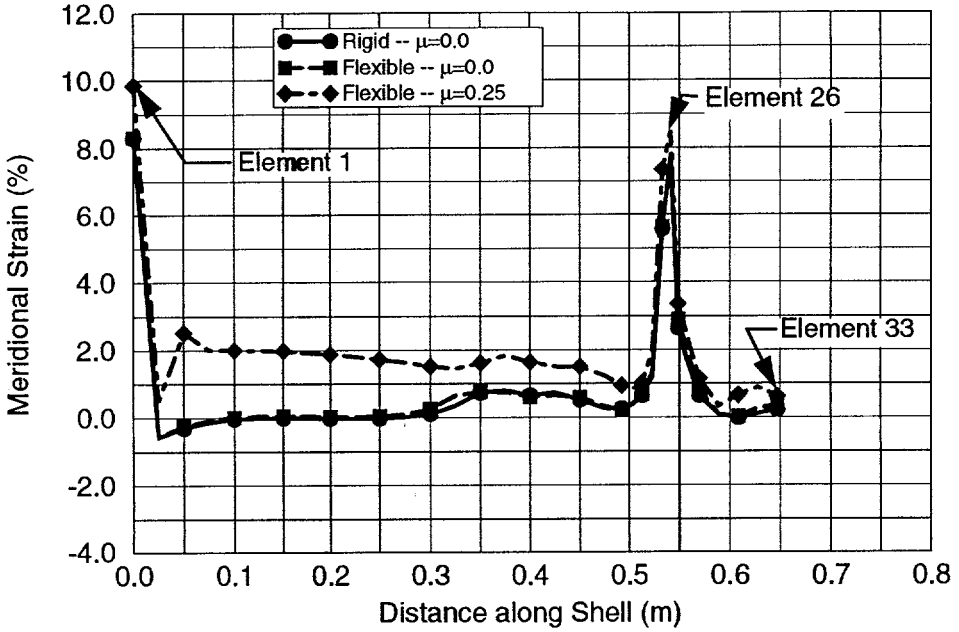

Figure 18. Meridional bending strain at the interior surface of the wet well wall at an internal pressure of 11.6MPa.

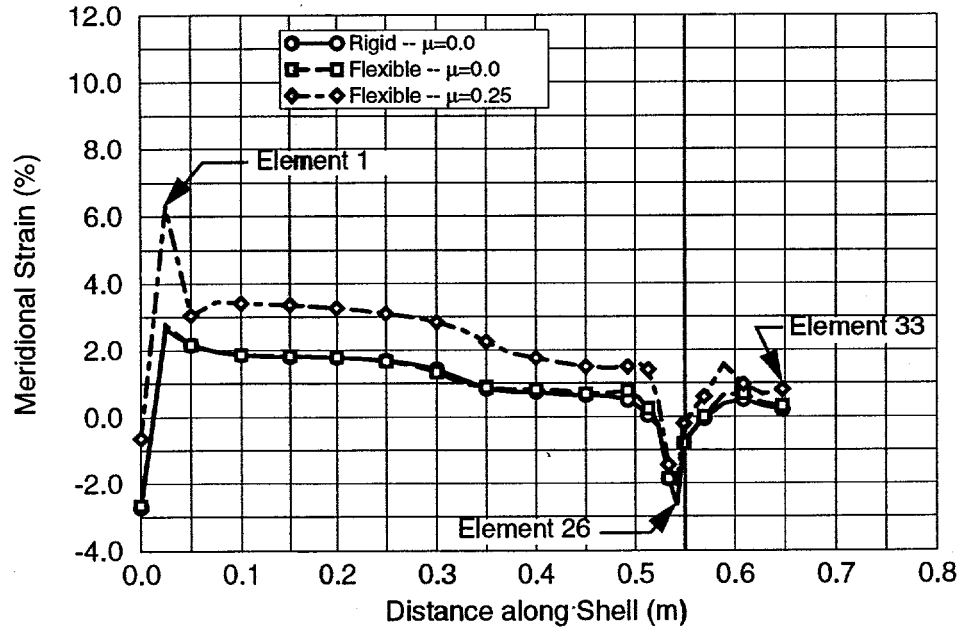

Figure 19. Meridional bending strain at the exterior surface of the wet well wall at an internal pressure of 11.6MPa.

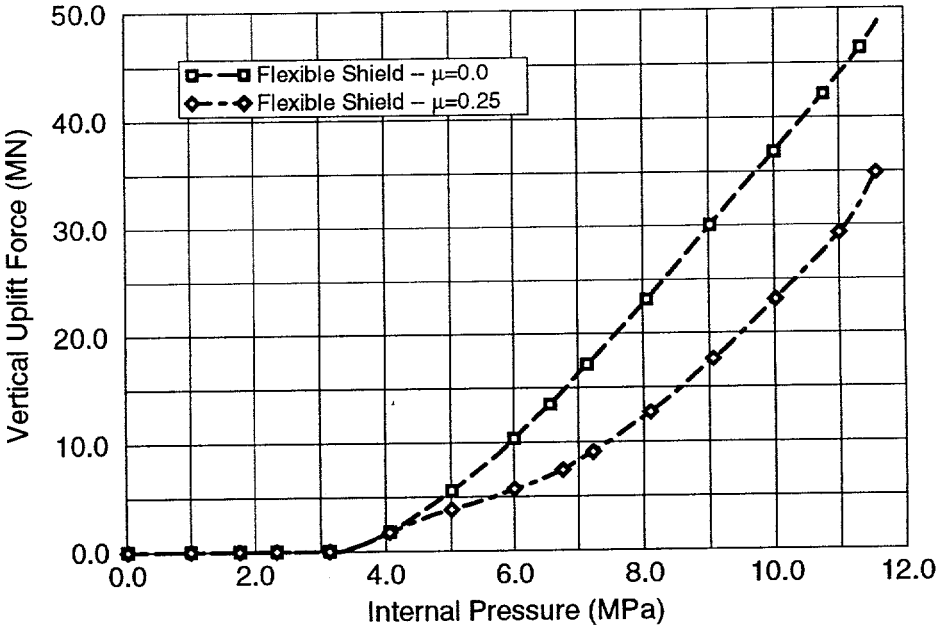

Figure 20. Uplift force on the ring support girder from the contact structure.